ACS OMEGA

Open Access

http://pubs.acs.org/journal/acsodf

Article

Integration of 2D Nanoporous Membranes in Microfluidic Devices

Niketa AK* and Shishir Kumar

Cite This: *ACS Omega* 2024, 9, 22305−22312

Read Online

ACCESS | Metrics & More | Article Recommendations | Supporting Information

ABSTRACT: 2D material-based membranes have emerged as promising candidates for next-generation separation technology due to their exceptional permeability and selectivity. Integration of these membranes into microfluidic devices has offered significant potential for improving the efficiency, throughput, and precision. However, designing compact and reliable microfluidic devices with membranes has many challenges, including complexities in membrane integration, analyte measurement, and contamination issues. Addressing these challenges is critical for unlocking the full potential of membrane-integrated devices. This paper proposes a systematic procedure for integrating membranes into a microfluidic device by creating a pore in the middle layer. Furthermore, an ion transport experiment is carried out across various stacked graphene and poly carbonate track etch membranes in an Ostemer-based device. The resulting device is capable of facilitating the concurrent measurement, a task that is cumbersome in standard macroscopic diffusion cells. The transparency and compactness of the microfluidic device allowed for the in situ and real-time optical characterization of analytes. The integration of microfluidic devices with 2D nanoporous membranes has enabled the incorporation of several analytical modalities, resulting in a highly versatile platform with numerous applications.

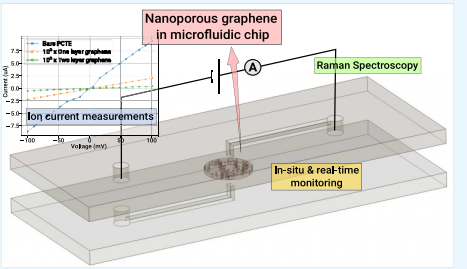

INTRODUCTION

Nanoporous membranes fabricated from 2D materials offer the potential for molecular-level filtration, identification, and sequencing, in many respects similar to biological pores.[1−5] A variety of biological nanopores use highly selective molecular filtering to regulate critical physiological functions. The possibility of mimicking them with 2D nanoporous membranes has led to a large body of work over the past decade.[6−9] The majority of separation-based experiments are conducted using either side-by-side diffusion cells or custom-made electrochemical cells with two reservoirs.[9−13] The macroscopic nature of the setup and the samples makes the reported findings average over a large number of pores, which may obscure the proper characterization of underlying physical phenomena near the vicinity of a nanopore. The investigation of isolated nanopores becomes even more crucial considering that the transport of molecules, ions, gases, or polymer strands have highly nonlinear dependence on features of the pores, e.g., their size or decoration.

On a practical level, the use of macroscopic implements limits the modality, scale, and efficiency of studies, resulting from the constraints of cost, time, and manual effort. For example, in diffusion cell analysis, membranes are analyzed one at a time, which limits suitability for in situ optical or spectral analysis of analytes.[14] A macroscopic area of the membrane, defined by the opening in the cell, is used for investigations, which either average out the effect of different-sized pores or need careful preparation to limit the statistical distributions. To reduce the predefined opening of the cell and mitigate potential leakage issues, it is necessary to explore alternative approaches to ensure secure connections to uphold the integrity of the setup. The bulk of the setup hinders integration and automation, besides being fiddly to work with the setup.[11,15,16]

The integration of nanopores into microfluidics devices can address most of these challenges elegantly and provide several significant benefits.[17−19] In microfluidic devices, the area of investigation of the membrane can be scaled down to reduce the statistical variance. Control over the opening of the microfluidic device allows for a high-precision study of the dynamics of translocation through the pores. Taken to the extreme, with proper adjustment of the areal density of pores, single pores could be investigated. The number of membranes can be scaled up at the same time, providing well-controlled data. Automation is inherent in microfluidic systems, overcoming the limitations posed by manual handling in microscopic setups.[20] The majority of microfluidic systems are amenable to high-quality optical and electrical investigation in situ, offering real-time and simultaneous measurement, which is impractical in diffusion cells.[21−26] The integration can extend to biochemical assays, facilitating a cohesive platform for applications too.

Received: February 21, 2024
Revised: April 22, 2024
Accepted: April 29, 2024
Published: May 8, 2024

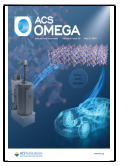

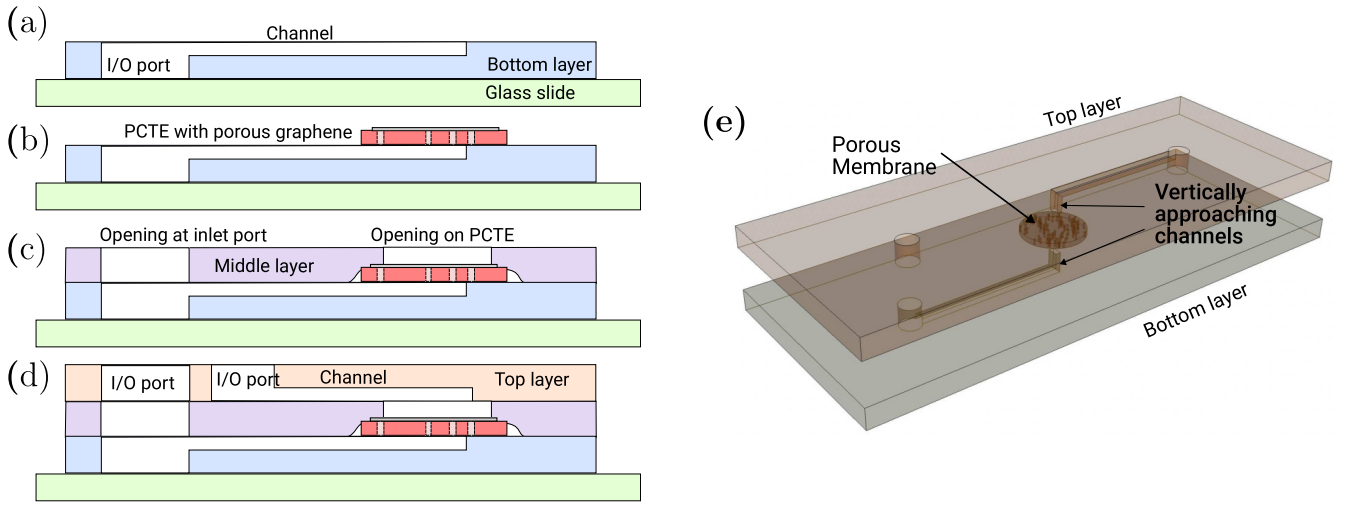

Figure 1. Fabrication process for the 3-layer microfluidic devices. (a) The bottom layer is placed on a glass slide, (b) followed by the placement of nanoporous graphene supported on a PCTE membrane. (c) The opening in the middle layer is aligned to the membrane, and finally, (d) the top layer is placed. All the layers are bonded at the end by heat curing. (e) 3D view of the device with vertically approaching channels on both sides.

Even with such impressive benefits, the fabrication process of integrating nanoporous membranes in microfluidic devices has limitations in the literature. Material compatibility restricts combinations of materials, leading to degraded adhesion and long-term robustness of the devices. The most popular material for microfluidics, polydimethylsiloxane (PDMS), lacks chemical robustness and is hydrophobic.[27−32] Along with material incompatibility, integrating a membrane into a microfluidic device is a challenging way for achieving the desired outcomes. In ref 33, researchers applied adhesive along the edges of the membrane. An alternative approach is to fabricate the membrane in situ after bonding the two layers of the microfluidic device.[34] Sacrificial layers,[35] 3D printing,[36] and ultrasonic bonding[37] have also been used, each with its own set of pros and cons (a comparison table can be seen in Supplementary Section 4). Common concerns include fabrication complexities, leakage issues, material restrictions, nonuniformities, residues, high costs, and contaminants, all of which can impede the proper functioning of the devices.[15,38−43]

This paper proposes a facile way to integrate 2D nanoporous membranes into a microfluidic platform to overcome fabrication and characterization-related challenges. Nanoporous graphene is supported on a relatively thick PCTE (polycarbonate track etched)membrane incorporated on Ostemer as a base material for fabrication of the device. Electrical measurements are carried out on several separate nanoporous graphene samples on a single device with on-device electrodes. The performance of the device is compared with the measurement obtained from diffusion cells. Furthermore, in situ optical microscopy and Raman spectroscopy are used to analyze dye diffusion through the graphene embedded in the device. The characterizations are performed without any special arrangements and bolster the versatility of the platform for multimodal analysis.

EXPERIMENTAL SECTION

Fabrication of Stacked Graphene on PCTE Membrane. *Synthesis of CVD Graphene on Cu.* Large-area single-layer graphene is synthesized in a homemade LPCVD on a Cu foil.[44] The procedure involves cleaning the copper foil (Sigma-Aldrich, 349208−33G) using deionized (DI) water, ethanol, and dry air. The clean copper foil is directly placed into a CVD chamber and anneals for 60 min at 1030 °C in a 100-standard cubic cm^3 (sccm) H_2 flow. Then, 10 sccm of CH_4 and 50 sccm of H_2 are introduced into the chamber to allow graphene growth. The growth time is set to 30 min to ensure full coverage of monolayer graphene. The copper foil is cooled to room temperature under the 100 sccm H_2 flow.

Transfer of Graphene to PCTE Membrane. Graphene is subsequently transferred onto a polycarbonate track-etched (PCTE, hydrophilic, Merck Millipore Ltd.) membrane with 200 nm pores that provide mechanical support using a direct transfer method to ensure minimal surface contamination.[10] At first, the graphene on the backside of the copper is removed by floating in a 0.1 M ammonium persulfate (APS) solution for 10 min. The remaining Cu foil, which has graphene on the top side, is rinsed in two consecutive water baths for 15 min each. After drying, the sample is placed on top of a glass slide, followed by a piece of PCTE membrane on top of the graphene, and a second glass slide is placed on top of the stack. The whole stack is lightly pressed using a roller. The PCTE membrane-supported graphene on copper is then transferred to a bath of 0.1 M APS etchant for full removal of the copper. The sample is then rinsed in a water bath, followed by a 50% ethanol/water bath, and finally air-dried.

Nanopore Formation in Graphene Membrane. Graphene membranes are exposed to air plasma in a tabletop Harrick plasma system (PDC-32G, maximum RF power of 18 W) at room temperature. The plasma treatment is performed for 4 s at a power of 10 W, under 100 sccm of air, at a pressure of 10 mbar.

Fabrication of Membrane Integrated Microfluidic Devices. The microfluidic devices are composed of bottom, middle, and top layers. The bottom and top layers had embedded channels, whereas the middle layer had cutouts to create an opening on top of membranes, which are sandwiched between the bottom and top layers. All of the layers are molded from the Ostemer 322 Crystal Clear polymer. The molds are made in PDMS, which is in turn molded by another mold made of Ordyl 330 dry film resist (DFR, 55 μm thick). Briefly, the DFR is laminated on a clean glass slide, and a Cr-

https://doi.org/10.1021/acsomega.4c01688
ACS Omega 2024, 9, 22305−22312

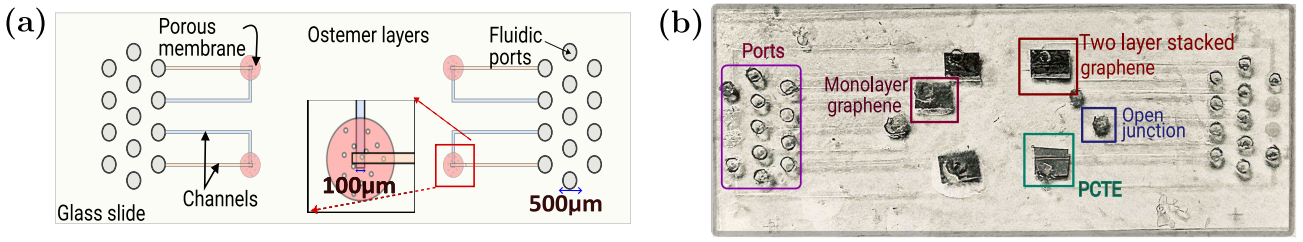

Figure 2. (a) Layout of the three.

coated glass mask is used to expose the DFR. It is then developed (developer XFB) and postbaked as per the vendor's guidelines. The slide with the Ordyl mold is kept at the bottom of a Petri dish, and premixed, degassed PDMS is poured on it. The PDMS is cured at 70 °C for 3 h on a hot plate and peeled off. The bump formed in the peeled PDMS mold is filled with premixed and degassed Ostemer 322 (1.09:1 mixture of parts A and B). After covering the surface of the poured Ostemer mix with a PET sheet, it is exposed to 1 min of UV-A (365 nm) radiation in a home-built exposure unit. The UV-cured Ostemer 322 layer is then peeled from the glass slide and placed upside down on top of another cleaned glass slide. This bottom layer had the channels on the side exposed to air in Figure 1(a). Pieces of PCTE membranes, having nanoporous graphene on them, are manually placed at the junctions of the bottom and top layer channels, as shown in Figure 1(b). A small drop of water is put on the membrane so that it conformally clings to the bottom layer due to capillary action. The water is allowed to dry, and the middle layer is placed on the devices with 100 μm holes aligned to the location of the PCTE membranes in Figure 1(c). The top layer, which is molded in the same manner as the bottom layer, is manually placed on the stack so that the ports and junctions in the bottom and top layers are aligned, as shown in Figure 1(d). The stack is pressed from the top and heat-cured on a hot plate at 110 °C for 1 h to yield the microfluidic devices. Detailed methods are described in Supplementary Section 1.

Electrical Characterization. The electrical measurements of the conduction of ions through the nanopores are done using the setup shown in Figure 5(a). Micropipettes are glued to the I/O ports of the microfluidic devices to provide space for the insertion of Ag/AgCl electrodes. The pipettes are then filled with 1 M KCl solution, and the electrodes are dipped in the pipettes. A source measure unit (SMU, Keithley 2460) is connected to the electrodes to apply voltage sweeps (10 mV increments within −0.1 and 0.1 V). The current flowing through the electrodes is recorded simultaneously. At the start of the measurements, both sides of the membrane are rinsed three times with 50% ethanol and water to wet the membrane. The same measurements are done in a diffusion cell (7 mL, Permegear Inc., 5.5 mm diameter opening), where membranes are sandwiched between two silicone layers (opening of 1 mm diameter), which are held and pressed between the two compartments of the diffusion cell. Both cells are then filled with KCl solution, and Ag/AgCl electrodes are used to apply an electric potential across the membrane.

Optical Characterization by Raman Spectroscopy. Raman spectra are collected using the WiTech 300R confocal Raman microscope using laser excitation at 532 nm. Optical microscopy is done with the same instrument using a 20X objective. The typical laser power and accumulation time are 28 mW and 5 s. An integration time of 12 s is used to accumulate a sufficient number of photons. The spectrometer provides a Raman spectrum over the range of 150 to 2000 cm^{-1} with a spectral resolution of better than 3 cm^{-1}.

RESULT AND DISCUSSION

Device Fabrication. Microfluidic devices are fabricated based on the descriptions provided in the methods sections. This work investigates the ion transport in stacked graphene configurations using a microfluidic device, replicating our findings in.[45] Microfluidic devices, with multiple channels featuring different membranes, simplify characterization compared to diffusion cells, where changing membranes and KCl concentrations are cumbersome. Rhodamine B is chosen as the analyte for optical characterization. Despite its health hazards, the dye is widely used in industry for coloring red chilies, which causes liver dysfunction or cancer. The device layout and photograph of the devices are shown in Figure 2(a) and Figure 2(b), respectively. Different porous membranes with open pores have been easily integrated into the single microfluidic device to investigate desired analytes. It is straightforward to place a large number of membranes on a single device, which is possible due to the small size of membranes and fluidic channels.

-layered microfluidic devices. The channels in the bottom and top layers are shown in blue and pink colors, respectively. Fluidic ports are also shown. The zoomed rectangle shows the PCTE membrane (red circle) placed between the three-layered device. (b) Photographs of the fabricated devices with different membranes are shown.

Ensuring Leakproof Flow in the Microfluidic Device. Integrating a porous membrane between two layers results in the creation of a pocket at the periphery of the membrane due to the deformation of the layers, as shown in Figure 3(a). This pocket forms because the surfaces of the layers only come into contact with each other after a certain distance from the edge of the membrane. As fluid channels in each layer intersect this pocket, an undesired path from one channel to another is formed. To mitigate this issue, two approaches are proposed to establish vertical contact between the channels.

The first approach involves ensuring that the membrane connects vertically to the channels in both layers and opens only within the periphery of the membrane, as depicted in Figure 3(b). The second method allows only one channel to vertically approach the membrane, as shown in Figure 3(c). We have implemented this latter approach in our design. Other methods to achieve the same goal are feasible. For instance, instead of inverting the bottom layer, as we did, it can be positioned with its channel side in contact with the substrate, and an additional hole can be created at the junction location. This alternative approach is simpler than our implementation.

Integration of porous membranes, even particularly thick ones, in microfluidic devices should have leak-tight interfaces

https://doi.org/10.1021/acsomega.4c01688
ACS Omega 2024, 9, 22305−22312

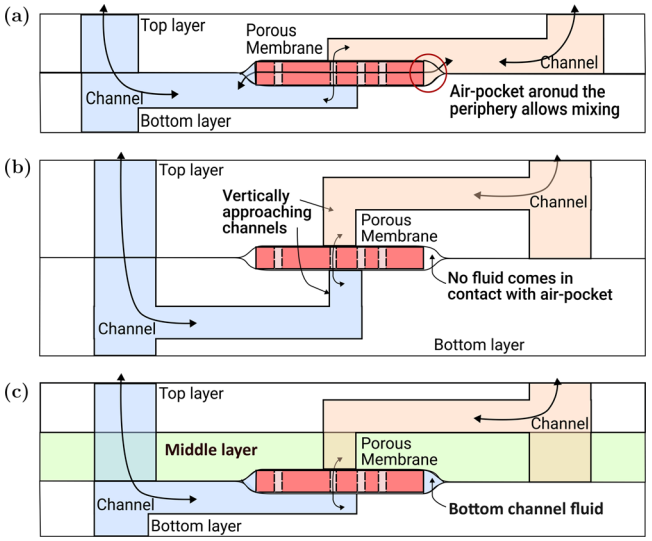

Figure 3. Schematics of the device: (a) A porous membrane sandwiched between two fluidic layers creates a pocket at the periphery of the membrane, which connects to the two fluidic channels, leading to leaks. (b) Allowing access to the nanopores via a vertical channel avoids the leak. (c) Similar to (b), but a single channel moved away from the membrane. Arrows denote the fluid flow path.

so that the desired flow occurs through the pores rather than through a parallel channel opened by the leak, as shown in Figure 4(a). For nanoporous materials, even a minute leak can swamp the flow characteristics of the nanopores (a detailed method of membrane integration is mentioned in Supplementary Section 2).

To assess the integrity of the membrane integration within the microfluidic device, the device is subjected to a prolonged leakage test. As prepared, the devices are submerged in ethanol for 30 min to ensure infusion into the channels. Subsequently, after removal of the device from ethanol, the inlet of one channel is filled with a blue solution of a food-coloring dye in ethanol. The channels are then observed under a microscope for any signs of leakage. After monitoring for several hours, the device did not show any leakage, as shown in Figure 4(b). In contrast, the same experiment done in devices without a middle layer, in which the air pocket at the edge connects the two channels, produced leaks at the edge and, consequently, the coloring of the other channel. This observation validates the effectiveness of the proposed method, affirming its capability to achieve a reliable and leak-proof seal.

In the experiment, the device design initially consisted of only eight locations for membrane placement. However, with a more compact layout design and tighter sizing of the membranes, it becomes feasible to analyze many more membranes simultaneously. In bioanalytical applications, the integration of membranes should not cause any major disruptions. After analysis of many single or multilayered graphene, no leakage or any other mode of failure has been observed in any of the devices tested. This emphasizes the robustness of the integration process and highlights its reliability for various applications.

ELECTRICAL AND OPTICAL CHARACTERIZATION

To evaluate the versatility of the microfluidic setup, both electrical and optical methods are utilized. In the electrical characterization process, the ionic current is measured across various membranes while the solution concentration. Subsequently, a comparison is made between the results obtained from both microfluidic and diffusion cell setups. Following this, optical characterization is conducted, which involves the Raman analysis of a health-hazard dye.

Microfluidic systems offer the distinct advantage of the integration of analytical capabilities in comparison with the standard diffusion cell setup, as shown in Figure 5(a). The compact devices and fluidic connections facilitate easy integration into other instruments, and in some cases (e.g., electrical analyses), the analytical apparatus can be integrated within the devices themselves. Moreover, with proper care, microfluidic devices are able to operate in almost any orientation. It is essential that the material of construction of the device should also not add any noise to the analysis while providing enough mechanical and chemical stability. Therefore, Ostemer is chosen as a material for the fabrication of devices.

Ionic transport through nanoporous graphene membranes embedded in both setups is analyzed to observe any changes in their behavior. In the microfluidic device setup as depicted in the schematic Figure 5(b), micropipets are affixed to the I/O ports of the devices and filled with electrolyte solutions. The electrodes are immersed into the inlet and outlet ports filled with electrolyte solution. The voltage is varied between −0.1 V

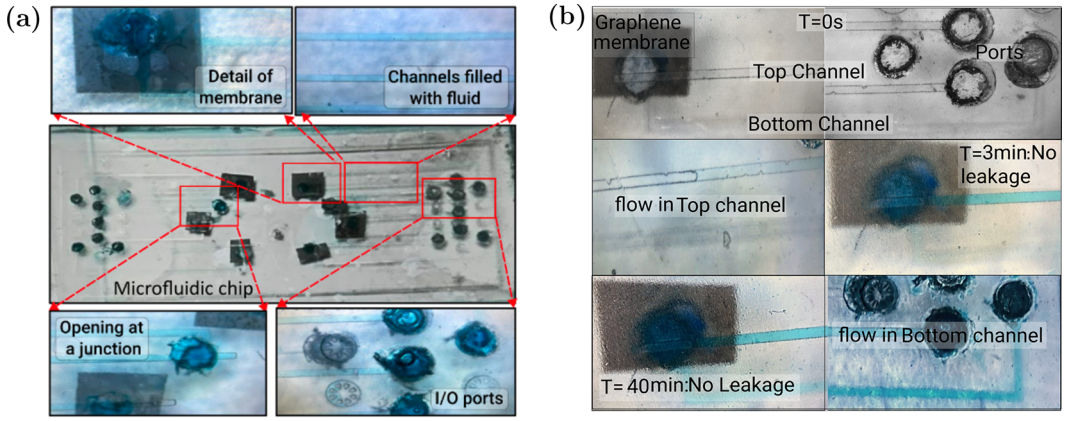

Figure 4. Photograph of the actual device after (a) the prolonged flow of blue-colored aqueous solution. (b) The liquid flows from the inlet port to the outlet port through the membrane with the time in the device (from top to bottom: 0 s, 3 min, and 40 min).

https://doi.org/10.1021/acsomega.4c01688
ACS Omega 2024, 9, 22305−22312

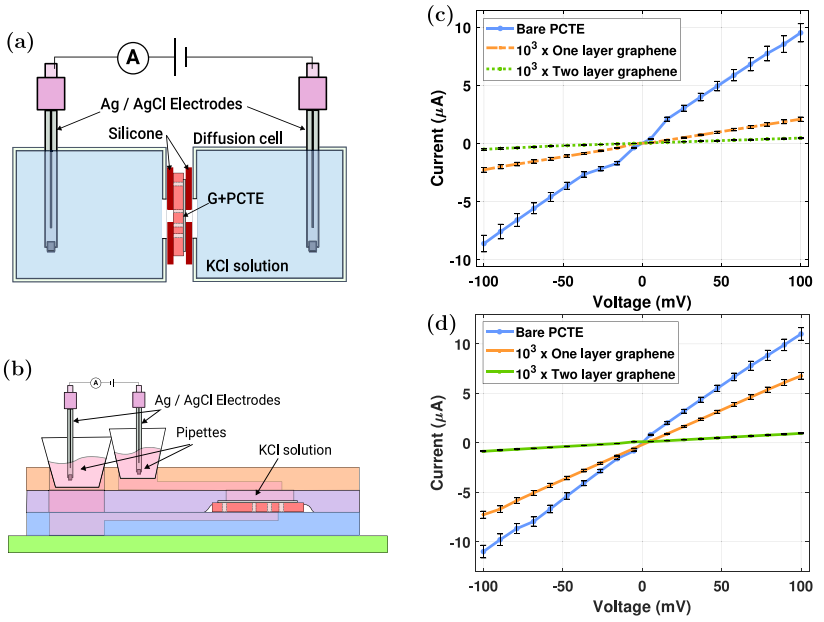

Figure 5. Schematic of an electrical measurement setup using (a) a conventional diffusion cell and (b) a microfluidic device. The electrical conductivity measurements from the two setups, (c) and (d) respectively, show the same characteristics. Error bars indicate the standard deviation of three repeated measurements for each data point.

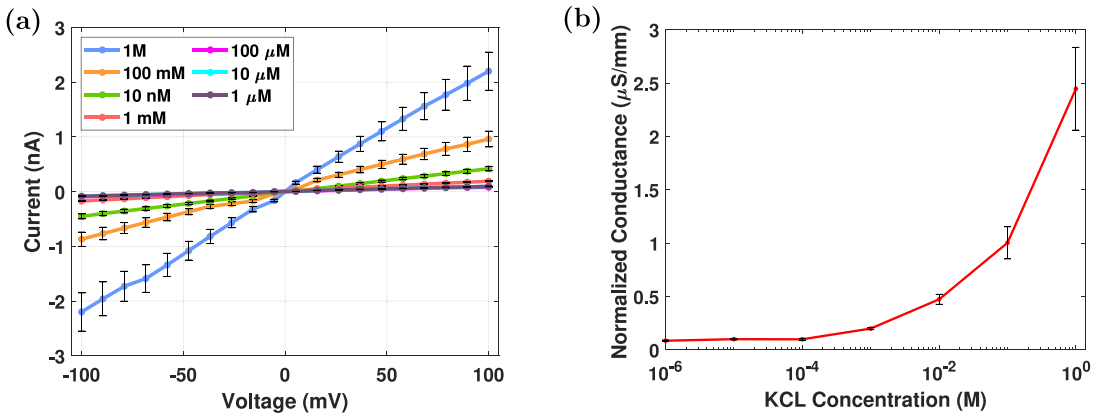

Figure 6. Electrical characterization: (a) VI curve of two-layer stacked graphene with 4 s of plasma exposure under a KCl concentration ranging from 1 μM to 1 M. (b) normalized area conductance with KCl concentrations. Error bars indicate the standard deviation of three repeated measurements for each data point.

to 0.1 V with 0.01 V steps across the membrane, and current is measured. Then, the experiment is carried out across the two channels. A bare PCTE and single- and two-layer nanoporous graphene (see Supplementary Section 3) are used. The concentration of the KCl solution is 10 mM. The same parameters are also used for measurements from a standard diffusion cell. In the case of a diffusion cell, the membrane needs to be changed, making it cumbersome to take measurements. The V−I characteristics in both cases are comparable, as depicted in Figure 5(c) and (d), indicating parity of usage.

In another set of experiments, ionic current measurements are performed across a two-layer stacked graphene membrane under different salt concentrations, ranging from 1 μM to 1M. The obtained V−I curve showed a linear behavior in Figure 6(a). The conductance plot with the KCl concentration revealed two distinct trends, as shown in Figure 6(b). A linear relationship is seen for concentrations above 10 mM. The conductivity remained almost constant below this concentration. The transition between these two regions occurs due to the dependence of debye length on salt concentration. As the salt concentration decreases, the electrical double layer on graphene starts approaching the nanopore dimensions so that the conduction is primarily governed by ions passing through the double layer to reach the other side.

More advanced characterization techniques are just as feasible with microfluidic devices as they are with electrical measurements. Specifically, given the resemblance of devices to a glass slide, albeit slightly thicker, they can be easily inserted into optical instruments. In contrast, optical spectroscopy in diffusion cells requires samples to be extracted, thereby limiting its operation. Rhodamine-B is selected as the analyte for optical characterization in the microfluidic setup. The bottom channel of the microfluidic device is filled with a solution containing 0.0001 M Rhodamine-B, while the top channel is filled with deionized (DI) water. Real-time, in situ characterization is performed by placing the device under the Raman spectroscope. The Raman signature of Rhodamine-B is

https://doi.org/10.1021/acsomega.4c01688
ACS Omega 2024, 9, 22305−22312

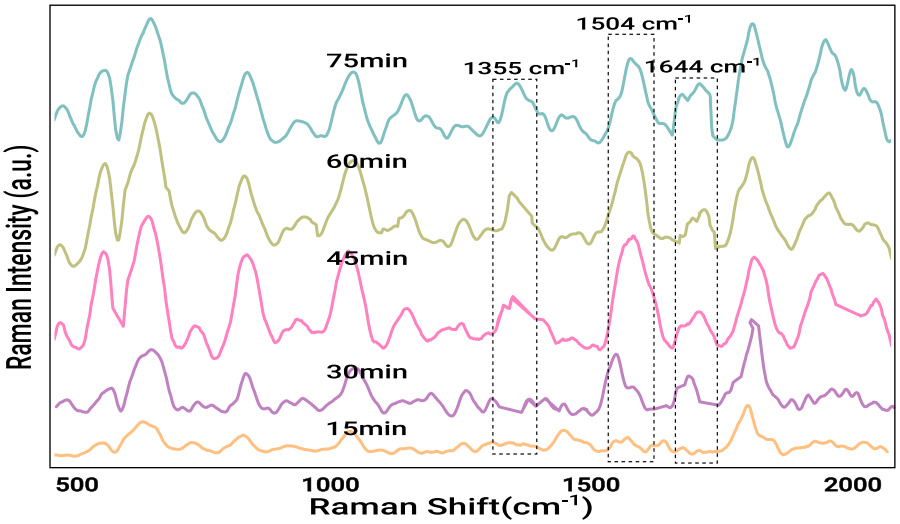

Figure 7. Temporal change in the Raman spectrum obtained from one location in the microfluidic channel in which Rhodamine B is diffusing. Its characteristic peaks (as marked) increased in intensity as time passed.

captured at 15 min intervals as it diffuses from the high-concentration channel to the low-concentration channel through the nanopores in graphene. These spectra, shown in Figure 7, exhibited characteristic peaks at 1355 cm^{-1}, 1504 cm^{-1}, and 1644 cm^{-1}. The increasing size of these peaks over time indicates the continuous diffusion of Rhodamine-B through the graphene nanopores into the adjacent channel. This method of characterization is sensitive enough to detect minute amounts of Rhodamine-B present in the system.

With the help of additional instrumentation, the basic functionality of the device can be leveraged for better characterization of ion movement across the nanopores. For example, with a precision stage, an areal map of the diffusing molecule can pinpoint the location of the pores, giving a direct measurement of density and indirect confirmation of the size of the pores. The latter can also be estimated and compared by using electrical measurements. Another possibility lies in the analysis of structured or masked membranes.

CONCLUSION

This paper proposes a fabrication technique to integrate diverse types of membranes into multichannel microfluidic devices to control molecular-level filtration and movement. A middle layer with a strategically positioned hole was introduced at the junction of both layers to prevent leakage along the membrane edge. The middle layer served as a barrier at the channel interface to ensure a leak-free flow of the fluid. The experimental results have shown that no leakage has occurred along the membrane edge, even after the fluid has been flowed for a prolonged duration. Additionally, the compactness and transparency of membrane-integrated microfluidic devices have enabled a wide range of characterization techniques for analytes. Specifically, electrical and optical methods have been used to evaluate the transit of ions and molecules through the membrane. The resulting platform has shown remarkable capability to integrate the highly efficient filtration of 2D nanoporous membranes into the bioanalysis pipeline of microfluidic systems, such as protein or DNA sequencing.

ASSOCIATED CONTENT

Supporting Information

The Supporting Information consists of: The Supporting Information is available free of charge at https://pubs.acs.org/doi/10.1021/acsomega.4c01688.

A detailed description of the fabrication process for a membrane-integrated microfluidic device; step-by-step procedure for the fabrication of an osteomer-based microfluidic device; photograph and schematics of the electrical setup for measuring the VI curve across the membrane; and comparison table of existing techniques for membrane integration in microfluidic devices

AUTHOR INFORMATION

Corresponding Author

Niketa AK − *Department of Electrical Engineering, Indian Institute of Technology Hyderabad, Sangareddy, Telangana 50228, India;* Present Address: Indian Institute of Technology Hyderabad, Kandi, Sangareddy, Telangana, India 502285; Email: ee19resch11010@iith.ac.in

Author

Shishir Kumar − *Department of Electrical Engineering, Indian Institute of Technology Hyderabad, Sangareddy, Telangana 50228, India;* Present Address: Indian Institute of Technology Hyderabad, Kandi, Sangareddy, Telangana, India 502285

Complete contact information is available at: https://pubs.acs.org/10.1021/acsomega.4c01688

Notes

The authors declare no competing financial interest.

ACKNOWLEDGMENTS

This research is supported by grant no. DST/NM/NT/2018/68 of Nanomission, India.

REFERENCES

(1) Koros, W. J.; Zhang, C. Materials for next-generation molecularly selective synthetic membranes. *Nature materials* **2017**, *16*, 289−297.

(2) Werber, J. R.; Osuji, C. O.; Elimelech, M. Materials for next-generation desalination and water purification membranes. *Nature Reviews Materials* **2016**, *1*, 1−15.
(3) Zhou, Z.; Guo, D.; Shinde, D. B.; Cao, L.; Li, Z.; Li, X.; Lu, D.; Lai, Z. Precise sub-angstrom ion separation using conjugated microporous polymer membranes. *ACS Nano* **2021**, *15*, 11970−11980.
(4) Liu, S.-H.; Zhang, D.; Fang, Y.-P.; Liang, Z.-X.; Zhao, Z.-K.; Chen, X.-C.; Yao, J.; Jiang, L. Topologically Programmed Graphene Oxide Membranes with Bioinspired Superstructures toward Boosting Osmotic Energy Harvesting. *Adv. Funct. Mater.* **2023**, *33*, No. 2211532.
(5) Yan, P.-P.; Chen, X.-C.; Liang, Z.-X.; Fang, Y.-P.; Yao, J.; Lu, C.-X.; Cai, Y.; Jiang, L. Two-dimensional nanofluidic membranes with intercalated in-plane shortcuts for high-performance blue energy harvesting. *Small* **2023**, *19*, No. 2205003.
(6) Liu, G.; Jin, W.; Xu, N. Two-dimensional-material membranes: a new family of high-performance separation membranes. *Angew. Chem., Int. Ed.* **2016**, *55*, 13384−13397.
(7) Peng, Y.; Yang, W. 2D metal-organic framework materials for membrane-based separation. *Advanced Materials Interfaces* **2020**, *7*, No. 1901514.
(8) Liu, P.; Hou, J.; Zhang, Y.; Li, L.; Lu, X.; Tang, Z. Two-dimensional material membranes for critical separations. *Inorganic Chemistry Frontiers* **2020**, *7*, 2560−2581.
(9) O'Hern, S. C.; Jang, D.; Bose, S.; Idrobo, J.-C.; Song, Y.; Laoui, T.; Kong, J.; Karnik, R. Nanofiltration across defect-sealed nanoporous monolayer graphene. *Nano Lett.* **2015**, *15*, 3254−3260.
(10) O'Hern, S. C.; Stewart, C. A.; Boutilier, M. S.; Idrobo, J.-C.; Bhaviripudi, S.; Das, S. K.; Kong, J.; Laoui, T.; Atieh, M.; Karnik, R. Selective molecular transport through intrinsic defects in a single layer of CVD graphene. *ACS Nano* **2012**, *6*, 10130−10138.
(11) O'Hern, S. C.; Boutilier, M. S.; Idrobo, J.-C.; Song, Y.; Kong, J.; Laoui, T.; Atieh, M.; Karnik, R. Selective ionic transport through tunable subnanometer pores in single-layer graphene membranes. *Nano Lett.* **2014**, *14*, 1234−1241.
(12) Surwade, S. P.; Smirnov, S. N.; Vlassiouk, I. V.; Unocic, R. R.; Veith, G. M.; Dai, S.; Mahurin, S. M. Water desalination using nanoporous single-layer graphene. *Nature Nanotechnol.* **2015**, *10*, 459−464.
(13) Jang, D.; Idrobo, J.-C.; Laoui, T.; Karnik, R. Water and solute transport governed by tunable pore size distributions in nanoporous graphene membranes. *ACS Nano* **2017**, *11*, 10042−10052.
(14) Sun, P. Z.; Yagmurcukardes, M.; Zhang, R.; Kuang, W. J.; Lozada-Hidalgo, M.; Liu, B. L.; Cheng, H.-M.; Wang, F. C.; Peeters, F. M.; Grigorieva, I. V.; Geim, A. K. others Exponentially selective molecular sieving through angstrom pores. *Nat. Commun.* **2021**, *12*, 7170.
(15) Schneider, S.; Gruner, D.; Richter, A.; Loskill, P. Membrane integration into PDMS-free microfluidic platforms for organ-on-chip and analytical chemistry applications. *Lab Chip* **2021**, *21*, 1866−1885.
(16) Fan, J.-B.; Luo, J.; Luo, Z.; Song, Y.; Wang, Z.; Meng, J.; Wang, B.; Zhang, S.; Zheng, Z.; Chen, X.; Wang, S. others Bioinspired microfluidic device by integrating a porous membrane and heterostructured nanoporous particles for biomolecule cleaning. *ACS Nano* **2019**, *13*, 8374−8381.
(17) Halldorsson, S.; Lucumi, E.; Gómez-Sjöberg, R.; Fleming, R. M. Advantages and challenges of microfluidic cell culture in polydimethylsiloxane devices. *Biosens. Bioelectron.* **2015**, *63*, 218−231.
(18) De Jong, J.; Lammertink, R. G.; Wessling, M. Membranes and microfluidics: a review. *Lab Chip* **2006**, *6*, 1125−1139.
(19) Harrison, D.; Li, P.; Tang, T.; Lee, W. Manipulation of biological cells and of DNA on-chip. *Anal. Methods Instrum.* **1996**, *96*, 147−149.
(20) Hediger, S.; Fontannaz, J.; Sayah, A.; Hunziker, W.; Gijs, M. Biosystem for ly culture and characterisation of epithelial cell tissues. *Sens. Actuators, B* **2000**, *63*, 63−73.
(21) Ly, K. L.; Hu, P.; Pham, L. H. P.; Luo, X. others Flow-assembled chitosan membranes in microfluidics: recent advances and applications. *J. Mater. Chem. B* **2021**, *9*, 3258−3283.
(22) Kratz, C.; Furchner, A.; Sun, G.; Rappich, J.; Hinrichs, K. Sensing and structure analysis by in situ IR spectroscopy: From mL flow cells to microfluidic applications. *J. Phys.: Condens. Matter* **2020**, *32*, No. 393002.
(23) Midelet, C.; Werts, M. H. Dielectrophoretically Modulated Optical Spectroscopy of Colloidal Nanoparticle Solutions in Microfluidic Channels. *Particle & Particle Systems Characterization* **2020**, *37*, No. 2000187.
(24) Chen, G.; Zheng, J.; Liu, L.; Xu, L. Application of microfluidics in wearable devices. *Small Methods* **2019**, *3*, No. 1900688.
(25) Konoplev, G.; Agafonova, D.; Bakhchova, L.; Mukhin, N.; Kurachkina, M.; Schmidt, M.-P.; Verlov, N.; Sidorov, A.; Oseev, A.; Stepanova, O.; et al. others Label-free physical techniques and methodologies for proteins detection in microfluidic biosensor structures. *Biomedicines* **2022**, *10*, 207.
(26) Zhong, Q.; Huang, X.; Zhang, R.; Zhang, K.; Liu, B. Optical sensing strategies for probing single-cell secretion. *ACS sensors* **2022**, *7*, 1779−1790.
(27) Łopacińska, J. M.; Emnéus, J.; Dufva, M. Poly (dimethylsiloxane)(PDMS) affects gene expression in PC12 cells differentiating into neuronal-like cells. *PLoS One* **2013**, *8*, No. e53107.
(28) Millet, L. J.; Stewart, M. E.; Sweedler, J. V.; Nuzzo, R. G.; Gillette, M. U. Microfluidic devices for culturing primary mammalian neurons at low densities. *Lab Chip* **2007**, *7*, 987−994.
(29) Regehr, K. J.; Domenech, M.; Koepsel, J. T.; Carver, K. C.; Ellison-Zelski, S. J.; Murphy, W. L.; Schuler, L. A.; Alarid, E. T.; Beebe, D. J. Biological implications of polydimethylsiloxane-based microfluidic cell culture. *Lab Chip* **2009**, *9*, 2132−2139.
(30) Sackmann, E. K.; Fulton, A. L.; Beebe, D. J. The present and future role of microfluidics in biomedical research. *Nature* **2014**, *507*, 181−189.
(31) Lee, J. N.; Jiang, X.; Ryan, D.; Whitesides, G. M. Compatibility of mammalian cells on surfaces of poly (dimethylsiloxane). *Langmuir* **2004**, *20*, 11684−11691.
(32) Ertel, S. I.; Ratner, B. D.; Kaul, A.; Schway, M. B.; Horbett, T. A. In vitro study of the intrinsic toxicity of synthetic surfaces to cells. *J. Biomed. Mater. Res.* **1994**, *28*, 667−675.
(33) Arayanarakool, R.; Le Gac, S.; van den Berg, A. Low-temperature, simple and fast integration technique of microfluidic chips by using a UV-curable adhesive. *Lab Chip* **2010**, *10*, 2115−2121.
(34) Orhan, J.-B.; Knaack, R.; Parashar, V.; Gijs, M. In situ fabrication of a poly-acrylamide membrane in a microfluidic channel. *Microelectronic engineering* **2008**, *85*, 1083−1085.
(35) Peeni, B. A.; Lee, M. L.; Hawkins, A. R.; Woolley, A. T. Sacrificial layer microfluidic device fabrication methods. *Electrophoresis* **2006**, *27*, 4888−4895.
(36) Ho, C. M. B.; Ng, S. H.; Li, K. H. H.; Yoon, Y.-J. 3D printed microfluidics for biological applications. *Lab Chip* **2015**, *15*, 3627−3637.
(37) Kistrup, K.; Poulsen, C. E.; Hansen, M. F.; Wolff, A. Ultrasonic welding for fast bonding of self-aligned structures in lab-on-a-chip systems. *Lab Chip* **2015**, *15*, 1998−2001.
(38) Zheng, S.; Lin, H. K.; Lu, B.; Williams, A.; Datar, R.; Cote, R. J.; Tai, Y.-C. 3D microfilter device for viable circulating tumor cell (CTC) enrichment from blood. *Biomed. Microdevices* **2011**, *13*, 203−213.
(39) Lee, K. S.; Ram, R. J. Plastic−PDMS bonding for high pressure hydrolytically stable active microfluidics. *Lab Chip* **2009**, *9*, 1618−1624.
(40) Petersen, N. J.; Jensen, H.; Hansen, S. H.; Foss, S. T.; Snakenborg, D.; Pedersen-Bjergaard, S. On-chip electro membrane extraction. *Microfluid. Nanofluid.* **2010**, *9*, 881−888.
(41) Mingareev, I.; Weirauch, F.; Olowinsky, A.; Shah, L.; Kadwani, P.; Richardson, M. Welding of polymers using a 2 μm thulium fiber laser. *Optics & Laser Technology* **2012**, *44*, 2095−2099.

https://doi.org/10.1021/acsomega.4c01688
ACS Omega 2024, 9, 22305−22312

(42) Luo, Y.; Zhang, Z.; Wang, X.; Zheng, Y. Ultrasonic bonding for thermoplastic microfluidic devices without energy director. *Microelectron. Eng.* **2010**, *87*, 2429−2436.
(43) Kappings, V.; Grün, C.; Ivannikov, D.; Hebeiss, I.; Kattge, S.; Wendland, I.; Rapp, B. E.; Hettel, M.; Deutschmann, O.; Schepers, U. vasQchip: a novel microfluidic, artificial blood vessel scaffold for vascularized 3D tissues. *Advanced Materials Technologies* **2018**, *3*, No. 1700246.
(44) Niketa, A.; Ikbal, M. A.; Kothapalli, S.; Kumar, S. An automated chemical vapor deposition setup for 2D materials. *HardwareX* **2021**, *9*, No. e00165.
(45) K, N. A.; Kumar, S. Ion Selectivity in Multilayered Stacked Nanoporous Graphene. *ACS Appl. Mater. Interfaces* **2024**, *16*, 5294−5301.

https://doi.org/10.1021/acsomega.4c01688
ACS Omega 2024, 9, 22305−22312